ELSEVIER

Physica C 280 (1997) 167–177

PHYSICA C

Growth and characterization of *a*-axis oriented $YBa_2Cu_3O_{7-x}$ thin films on (100) $LaSrGaO_4$ substrates

D. Fuchs [a,*], E. Brecht [a], P. Schweiss [a], I. Loa [b], C. Thomsen [b], R. Schneider [a]

[a] *Forschungszentrum Karlsruhe, Institut für Nukleare Festkörperphysik, POB 3640, D-76021 Karlsruhe, Germany*
[b] *TU Berlin, Institut für Festkörperphysik PN 5-4, Hardenbergstrasse 36, D-10623 Berlin, Germany*

Received 1 March 1997; accepted 25 April 1997

Abstract

We grew *a*-axis oriented $YBa_2Cu_3O_{7-x}$ thin films on (100) oriented tetragonal single crystalline $LaSrGaO_4$ substrates by inverted cylindrical magnetron dc sputtering. $PrBa_2Cu_3O_{7-x}$ thin films deposited in situ by rf sputtering were used as template layers. The growth of the films was studied by X-ray diffraction, high-resolution transmission electron microscopy and Raman spectroscopy. Their surface morphology has been characterized by atomic force microscopy. In addition, normal state and superconducting transport properties were measured on patterned films by use of a four-probe arrangement. The film composition was controlled by energy-dispersive X-ray analysis and Rutherford backscattering spectrometry that also enabled the determination of the film thickness. We obtained $YBa_2Cu_3O_{7-x}$ films with pure *a*-axis growth and full *c*-axis in-plane alignment with the orientational relationship of (010) YBCO||(010) LSGO and (001) YBCO||(001) LSGO. The crystalline anisotropy is also reflected in the transport properties where the resistivity and j_c anisotropies parallel and perpendicular to the *ab*-plane reach 18 and 7, respectively, at 100 K. T_c amounts to 90.5 K and j_c parallel to the *ab*-plane is 1.3×10^5 A/cm^2. The film surfaces showed large grains with a size of 500×170 nm^2 but no significant outgrowths resulting in a mean surface roughness of $R_a = 5$ nm. Grain boundaries, including antiphase boundaries in the *b*-direction and stacking fault boundaries in the *c*-direction have been observed and are discussed with respect to their influence on the anisotropic transport. © 1997 Elsevier Science B.V.

1. Introduction

Extensive efforts have been made to prepare high-quality high T_c thin films for developing superconducting devices. $YBa_2Cu_3O_{7-x}$ (YBCO) films with *a*-axis orientation are considered to be the most promising route for the fabrication of sandwich-type Josephson junctions [1–5] because of their much longer coherence length along the CuO_2 (*ab*) planes (1.2–1.5 nm versus 0.1–0.3 nm along the *c*-axis) and a very smooth surface on the atomic scale [6,7].

a-axis films were grown first on cubic perovskite substrates such as (100) $LaAlO_3$, (100) $SrTiO_3$ and MgO [7–10], which are also used for the growth of *c*-axis films. These films often showed a rather poor transition temperature T_c of less than 85 K and a strong *bc* twinning [10].

The twinning can be avoided by using tetragonal substrates with a rectangular surface cell like

* Corresponding author. Tel: +49 7247 82 3985; Fax: +49 7247 82 4624; e-mail: dfuchs@infp.fzk.de

PII S0921-4534(97)00182-2

$CaNdAlO_4$ [11], Nd_2CuO_4 [12], $LaSrAlO_4$ [13] or $LaSrGaO_4$ (LSGO) [14,15], leading to an in-plane alignment of the *c*-axis along the best matching direction [16–18]. The most promising substrate for the growth of high-quality *a*-axis films with a full *c*-axis in-plane alignment is (100) LSGO, recently used by several other groups [14,16–21]. LSGO has a K_2NiF_4-type crystal structure with $a = 0.3843$ nm and $c = 1.2681$ nm [22]. Among the tetragonal substrates it has two important benefits: firstly, the lattice mismatch between its shorter lattice constant and the *a* lattice constants of YBCO and $PrBa_2Cu_3O_{7-x}$ (PBCO) is only $+0.6\%$ and -0.7%, respectively; secondly, the thermal expansion coefficients in *b*- and *c*-direction are nearly the same: 10.05 ppm/K for LSGO and 10 ppm/K for YBCO along the *a*/*b*-direction and 18.94 ppm/K for LSGO and 17 ppm/K for YBCO along the *c*-direction [15,21], which leads to a minimum of strain and cracks in the film during heating or cooling.

However, obtaining T_cs as high as in *c*-axis films deposition at high substrate temperatures of 750° to 800°C is required which leads, on the bare substrate, to a change of the growth orientation towards *c*-axis growth [23]. The transition temperature where the preferential YBCO orientation changes from *a*-axis to *c*-axis growth also depends on the lattice mismatch of the substrate material [24].

One possible technique that enables the deposition of pure *a*-axis oriented YBCO films at relatively high temperatures is the use of a template like YBCO (self-template) [25,26], cubic YBCO/PBCO [27] or PBCO [10,17–19,28,29] (heterotemplate).

The method can be described as follows: first, the template is deposited at low temperatures of 640°C to 750°C to obtain pure *a*-axis growth of the template layer. The deposition temperature depends in detail on the specific template and substrate material; second, the substrate temperature is raised up to 750°C to 800°C, which does not affect the growth orientation of the template; last, due to the much better lattice matching with the template material, pure *a*-axis YBCO films can be deposited at those high temperatures without any change of the growth direction.

In this paper we report on the growth of thin *a*-axis oriented, *c*-axis in-plane aligned YBCO films on (100) LSGO substrates using the heterotemplate technique with PBCO as a template. We have studied the crystalline quality of the PBCO templates and YBCO films by X-ray diffraction (XRD), high-resolution transmission electron microscopy (TEM), atomic force microscopy (AFM) and Raman spectroscopy. The film composition and thickness have been controlled by electron-dispersive X-ray analysis (EDX) and Rutherford backscattering spectrometry (RBS). The transport properties have been characterized by four-point measurements of the resistivity and the critical current density on thin patterned bridges with a length of 400 μm and a width of 100 μm, one being parallel to (010) LSGO and the other being parallel to (001) LSGO.

2. Template preparation and characterization

To optimize the epitaxial growth of our PBCO templates with respect to pure *a*-axis growth, we have deposited films at temperatures T_s between 650°C and 800°C using an inverted cylindrical magnetron (ICM) sputter gun driven in the rf mode and equipped with a stoichiometric 123-PBCO target. The substrates were glued onto the surface of a heater block using silver paste for good thermal contact. The quoted T_s values are those of the heater block measured with a thermocouple. The deposition was carried out at a total pressure of 0.1 mbar in an 1 : 1 argon–oxygen mixture, 100 W rf power (f = 13.56 MHz) and a target–substrate distance of 3 cm, resulting in a deposition rate of about 0.2 nm/s. After deposition the samples were cooled down to room temperature in 0.6 bar O_2 by turning off the heater.

In order to study the growth orientation as a function of the substrate temperature, T_s, Θ–2Θ scans were performed by using a standard two-axes diffractometer with $CuK\alpha_1$ radiation. Only ($h00$) and ($00l$) reflections of PBCO were observed. To determine quantitatively the volume fraction of *a*-axis oriented grains ω-scans at the (100) and (005) reflections were carried out. The ratio of the measured integral intensities weighted by theoretical structure factors and a geometrical factor provides the *a*-axis volume fraction. A four-circle diffractometer with $MoK\alpha_1$ radiation was also used to determine the PBCO lattice parameters. Within the

experimental resolution of our diffractometers, (h00) and (0k0) reflections with same indices $h = k$ could not be resolved and were only observable as one broadened peak in the Θ–2Θ scan. The measurements revealed a pseudo-tetragonal structure with lattice parameters $a \approx b = 0.391$ nm and $c = 1.187$ nm without any significant dependence on T_s. The lattice parameters of bulk PBCO ($PrBa_2Cu_3O_{6.8}$) are $a = 0.3870$ nm, $b = 0.3934$ nm and $c = 1.173$ nm [29].

The a-axis content as a function of the deposition temperature, T_s, is shown in Fig. 1(a). Up to $T_s = 775$°C the films grow almost purely a-axis oriented. Above this temperature admixtures of c-axis oriented grains start to grow. The mosaic spread of the a-axis grains in the direction perpendicular to the substrate surface was studied by measuring the rocking curves of the (100) reflections. The full width at half maximum (FWHM) of the ω-scans versus T_s is plotted in Fig. 1(b). A minimum of 0.6° appears in the temperature range from 725°C to 750°C. This

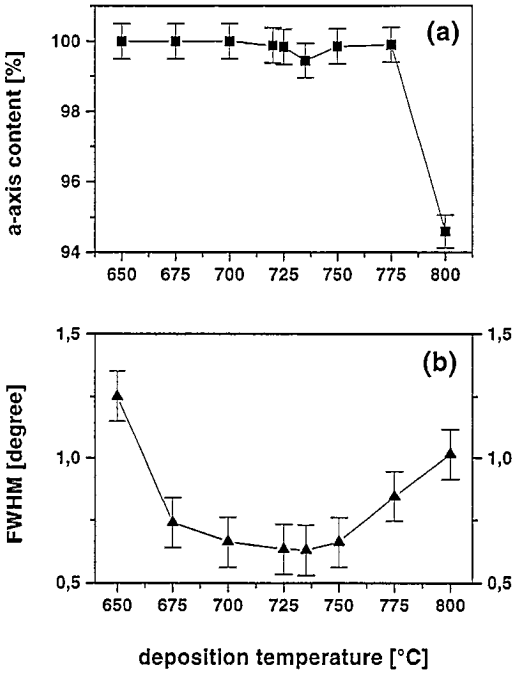

Fig. 1. (a) a-axis content of the PBCO templates as a function of the deposition temperature T_s. (b) FWHM of the rocking curves measured at (100) reflections versus T_s.

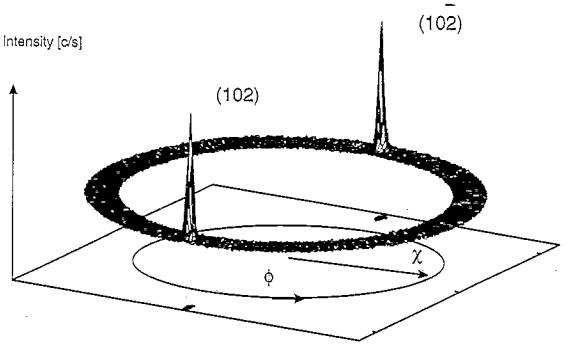

Fig. 2. Polar plot of ϕ- and χ-scans at the (102) reflection of a PBCO film deposited at 750°C demonstrating the in-plane texture.

value is quite large for epitaxially grown 123-cuprate thin films, but enhanced mosaic spreads of 0.45° to 0.7° seem to be typical for cuprate thin films on LSGO for the growth orientations (100), (001) and (110) [14,19,30].

The in-plane orientation of the films was investigated by ϕ- and χ-scans at the (102) reflection of PBCO and the (103) reflection of LSGO using a four-circle diffractometer. Fig. 2 demonstrates the ϕ- and χ-scans on the (102) reflection of a PBCO film deposited at $T_s = 750$°C. Only two strong peaks at $\phi = 0°$ and $\phi = 180°$ ($\chi = 33.2°$) corresponding to the (102) and (10$\bar{2}$) reflection of PBCO are observed. The FWHM of the reflections in ϕ and χ is 1.6° which can be taken as the mosaic spread of the grains in and perpendicular to the film surface along the (001) direction of PBCO, respectively.

No significant intensities at $\phi = 90°$ and $\phi = 270°$ originating from grains which are in-plane misoriented by 90° due to bc twinning were detected. The degree of c-axis in-plane alignment, given by the ratio of the intensities at $\phi = 0°$ and $\phi = 90°$, is larger than 98% within the range of the deposition temperature T_s of 700°C to 775°C. ϕ-scans at the (103) reflection of LSGO reveal an orientational relationship of (001) PBCO‖(001) LSGO and (010) PBCO‖(010) LSGO.

The microstructure of the films was investigated by high-resolution TEM. The growth quality was nearly perfect within a grain. Domains showing a bc twinning could scarcely be detected, well in agreement with our results from XRD measurements.

However, one dominant defect structure is shown in Fig. 3. Neighbored domains nucleate out of registry, resulting in antiphase boundaries (APBs) along the *b*-direction and in stacking faults (SFs) along the *c*-direction. The APBs mostly show shifts of $c/3$ and $c/6$. A more precise determination of the row spacings along the (001) direction allows an identification of Ba, Pr and Cu atoms. In the case of an APB we found that along the (010) direction the Ba rows end up at Pr rows and the Cu rows end up at Cu rows, remaining undisturbed.

Miyazawa et al. have suggested that these planar defects are correlated with the cobbled substrate surface of (100) LSGO [31]. Within their "atomic graphoepitaxy" growth model for *a*-axis oriented and *c*-axis in-plane aligned YBCO films on (100) LSGO [12], they modelled the appearance of such defects in terms of atomic steps on the cobbled surface.

An alternative explanation for the appearance of APBs which seems to be more likely from our results is a disorder of Ba and Pr cations. This is supported by the finding that the defects are randomly distributed and do not show any systematic occurrence with respect to the atomic structure of the substrate material.

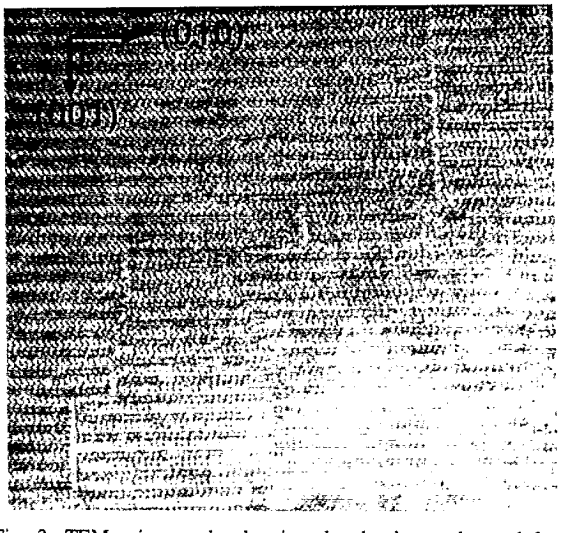

Fig. 3. TEM micrograph, showing the dominant planar defect structures, antiphase boundaries along (010) and stacking faults along (001), of PBCO templates grown on (100) LSGO.

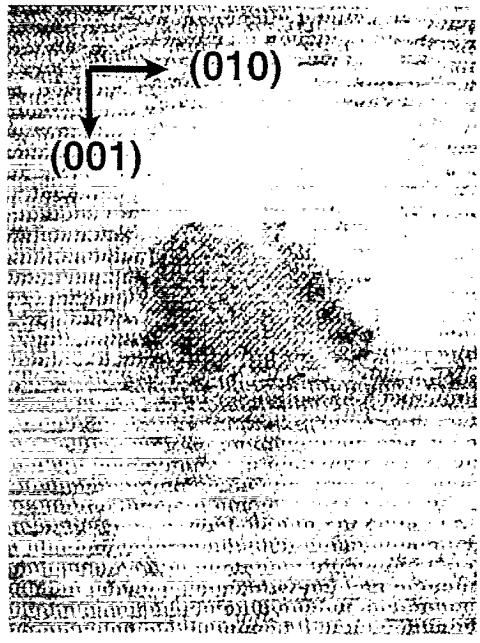

Fig. 4. TEM micrograph of a PBCO region, showing a grain of epitaxial grown $Pr_2Ba_4O_{7-x}$.

Besides planar defects we also observed one prominent impurity phase shown in Fig. 4. From electron diffraction and XRD measurements we obtained a cubic body centered (bcc) structure and a lattice constant of $a = 0.435$ nm for this phase. The composition was analyzed by EDX revealing a composition of $Pr_2Ba_4O_{7-x}$ (PBO). In addition to TEM micrographs ϕ-scans at the (220) and (211) reflections of PBO and at the (102) reflection of PBCO also showed that PBO grows epitaxially within the bulk PBCO matrix. The typical grain size of the PBO grains is about 9×9 nm^2, as derived from Fig. 4.

A necessary prerequisite for the growth of thin and smooth YBCO films on templates is that the underlying template layer has a smooth surface. Therefore, we characterized the surface morphology of our PBCO templates by AFM. Fig. 5 displays an AFM image of a PBCO template deposited under optimized conditions with respect to crystalline quality.

A prominent feature is the larger grain size of 500 nm along the (010) direction compared to 190 nm

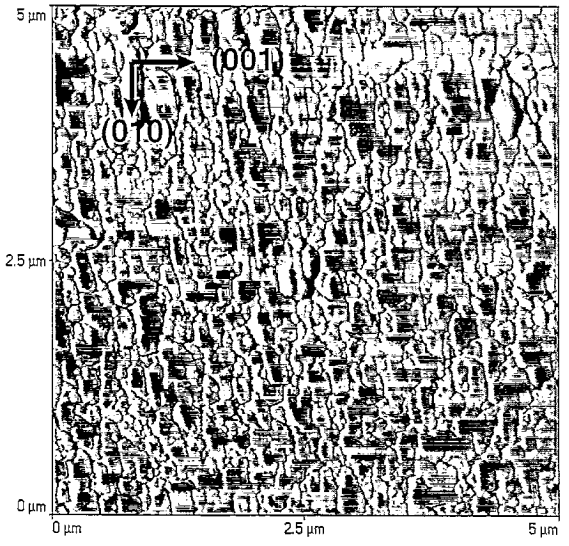

Fig. 5. AFM image of a PBCO template deposited under optimized conditions with respect to crystalline quality.

along the (001) direction resulting in an aspect ratio of nearly 3. This observation can be well understood in the frame of growth models considering thermodynamic and kinetic arguments [32–35]. *a*-axis growth, which is in contrast to *c*-axis growth kinetically preferred, because it proceeds by direct material addition, occurs preferentially under supersaturation conditions suppressing the mobility of the atoms and therefore the migration length [23,36]. Supersaturated deposition conditions favor therefore a higher growth rate along the (100) and (010) direction than along the (001) direction.

The mean surface roughness, R_a, of the films, defined as the average deviation from the mean line within the assessment length of 5 µm, was 5 nm. The surfaces were homogeneously smooth and did not show any remarkable outgrowths.

We also investigated the film quality as a function of the film thickness as determined by RBS. A slight increase of the *c*-axis content below a film thickness of 100 nm was observed. In addition, the FWHM of the rocking curves on (100) reflections increased strongly below a film thickness, d, of 50 nm from 0.6° at $d = 60$ nm to 2.5° at $d = 20$ nm. This is a hint for a change of the growth direction in the vicinity of the substrate surface towards pure *c*-axis or mixed *c*/*a*-axes growth orientation of the first layers on the substrate.

Interfacial *c*-axis oriented layers in *a*-axis oriented 123-cuprate films have been detected by other groups as well even at relatively low deposition temperatures [20,37–39]. A strong dependence on the specific substrate material and deposition rate has also often been observed.

Regarding the lattice mismatch between the *c*-axis lattice parameter of LSGO and the *b* and *c* lattice constants of PBCO, a *c*-axis oriented growth direction should be indeed favored over an *a*-axis growth direction, because $3 \times b$ fits better to the *c*-axis parameter of LSGO than the *c* lattice constant of PBCO. The results give rise to the assumption that in the case of LSGO as substrate material the lattice mismatch is the dominant parameter for the growth mode in the initial stage of the film growth on the bare substrate.

In order to avoid any possible negative influence with respect to the epitaxial growth of the overlying YBCO films, we prepared our templates with a thickness larger than 100 nm, typical 125 nm, to ensure pure *a*-axis growth of YBCO.

3. Growth and properties of *a*-axis oriented YBCO films

YBCO films were deposited at temperatures T_s between 650°C and 800°C on a PBCO template by

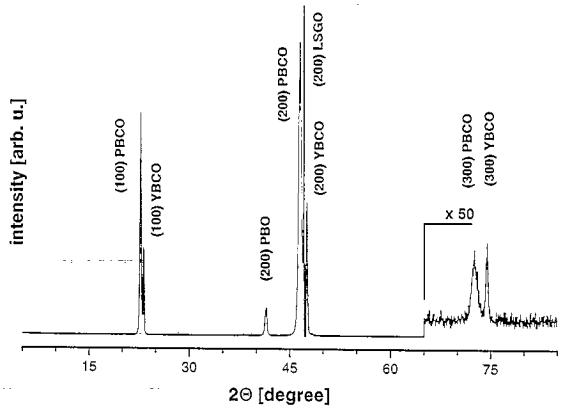

Fig. 6. $\Theta/2\Theta$-scan of an optimized YBCO/PBCO sample on (100) LSGO.

using an inverted cylindrical magnetron (ICM) sputter gun driven in the dc mode and equipped with a stoichiometric 123-YBCO target. The template has been deposited at $T_s = 750°C$ as described before. The deposition of YBCO was carried out at a total pressure of 0.6 mbar in an 1 : 1 argon–oxygen mixture, 100 W dc power and a target–substrate distance of 3 cm, resulting in a deposition rate of about 0.2 nm/s. After the preparation the samples were cooled down to room temperature in 0.6 bar O_2 by turning off the heater.

Fig. 6 shows a Θ–2Θ-scan of a YBCO/PBCO sample on (100) LSGO where the YBCO film was deposited at $T_s = 750°C$. The figure demonstrates the a-axis orientation of YBCO. Besides the (h00) reflections of PBCO, the (200) reflection of PBO and LSGO, only (h00) reflections of YBCO are observable. The (300) reflection of YBCO at $2\Theta = 74.5°$ is much sharper than that of PBCO which may be, on the one hand, broadened due to a stronger variation of the a lattice constant inducing strain into the film. If the structure of PBCO deviates only slightly from tetragonal symmetry in a way that makes it difficult to distinguish between the a and b lattice constants within our experimental resolution, the broadening of the (300) reflection could be induced, on the other hand, by a mixed a/b-axes growth orientation. A peak broadening for mixed a/b growth has been reported in Ref. [40].

For the lattice parameters of YBCO we obtained $a = 0.382$ nm, $b = 0.390$ nm and $c = 1.171$ nm, well matching with those of bulk YBCO ($a = 0.382$ nm, $b = 0.388$ nm and $c = 1.167$ nm) [41].

Fig. 7 shows the a-axis content of the YBCO films with and without PBCO template as a function of T_s. For the determination of the a-axis content, we used the intensities of the (100) and (005) reflections, measured by ω-scans as described before. Without template pure a-axis growth stops at about 675°C turning into a mixed a/c-axes growth. Pure c-axis orientation is reached at about 725°C. Using a template YBCO films with an a-axis content larger than 98% can be obtained up to $T_s = 750°C$ with only a slight decrease of the a-axis content above this temperature. Even at 800°C a-axis growth orientation still dominates and is larger than 90%. The results demonstrate impressively the influence of the PBCO template on the growth orientation of YBCO.

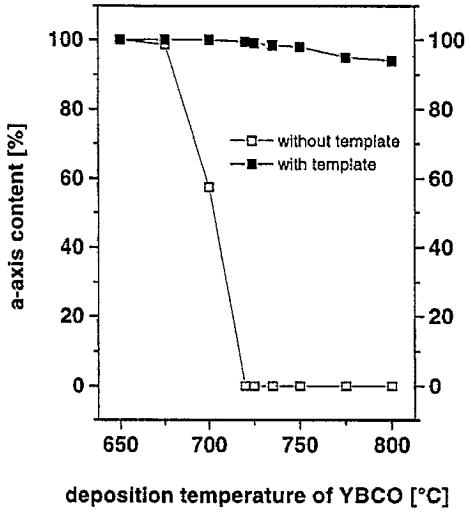

Fig. 7. a-axis content of YBCO films deposited with and without PBCO template on (100) LSGO versus T_s.

The in-plane orientation of a-axis oriented YBCO films was studied by ϕ-scans at the (102) reflection of YBCO and PBCO and the (103) reflection of LSGO, displayed in Fig. 8. The degree of in-plane alignment is given by the ratio of the measured integral intensities at $\phi = 90°$ and $\phi = 180°$,

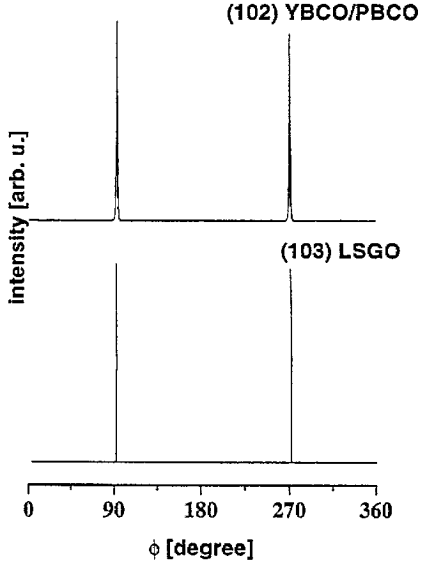

Fig. 8. ϕ-scan at the (102) reflection of a-axis oriented YBCO/PBCO (top) and at the (103) reflection of (100) LSGO (bottom).

$I_{\phi=90°}/(I_{\phi=90°}+I_{\phi=180°})$. Within the experimental resolution of our four-circle diffractometer we could not resolve (102) reflections of YBCO and PBCO. Therefore, measurements of the in-plane alignment were only carried out by XRD on YBCO films having a thickness larger than or equal to that of the PBCO template to ensure a sufficient sensitivity regarding the intensity. We observed full in-plane alignment, larger than 98%, depending only slightly on T_s. From Fig. 8, one can also obtain the orientational relationship between YBCO, template and substrate: (001) YBCO‖(001) PBCO‖(001) LSGO. The *b*-axes of LSGO, PBCO and YBCO are also oriented parallel to each other.

In-plane alignment and substrate-induced defects were studied in detail by spatially resolved Raman spectroscopy on YBCO films with a thickness smaller than 50 nm. The Raman spectra were recorded in $[a(bb)\bar{a}]$ backscattering geometry at ambient temperature using the 514 nm line of an Ar^+ laser. The laser beam was focused by a 100× microscope objective, providing a spatial resolution of better than 1 μm. To avoid damage of the sample, the excitation laser power was kept below 1 mW. By means of a scanning mirror and detection with a CCD array detector, complete line scans could be recorded at once. Series of such line scans were used to build up the complete 2-dimensional spectral information.

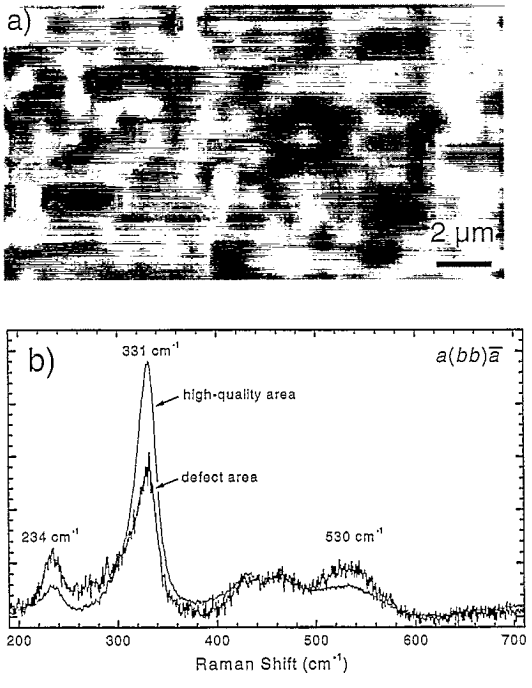

Fig. 9. (a) Spatially resolved intensity distribution of the 331 cm^{-1} Raman mode of an *a*-axis oriented YBCO film. Defect areas due to dips in the substrate appear as dark spots; (b) Raman spectra of the defect and high-quality regions. The spectra are averaged over different numbers of points, thus showing a better signal-to-noise ratio for the high-quality region.

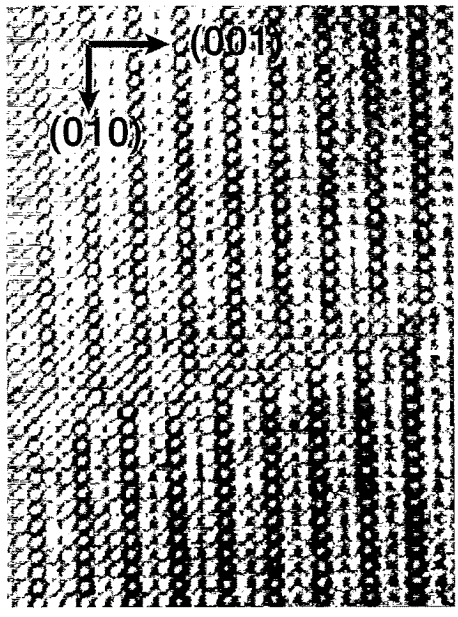

Fig. 10. TEM micrograph of a YBCO region which contains antiphase boundaries.

Fig. 9(a) depicts the spatial distribution of the intensity of the Raman mode at 331 cm^{-1} (O_{II}–O_{III} out-of-phase mode) for an area of 18 by 10 μm (30 × 14 spectra). It shows some small areas of low intensity (dark spots) within a rather homogeneous distribution. Fig. 9(b) compares a Raman spectrum of the dark spots with one of the high-quality region. In addition to the reduced intensity of the 331 cm^{-1} mode the well-known defect modes at 234 and 530 cm^{-1} appear, indicating that the irregularities are not caused by misalignment but by growth defects. By comparison with conventional microscopic images of both the substrate and the film, these areas can be associated with dips in the substrate produced by the preceding etching process, which leads to defects in the YBCO film leaving the orientation, however, intact.

The *bc* in-plane alignment of the film could be confirmed in a similar fashion. The Raman mode at 500 cm^{-1} (O_{IV} displacement) appears with maximum intensity in $[a(cc)\bar{a}]$ geometry, i.e. with both the incident and analyzing polarization parallel to the *c*-axis. The spatially resolved Raman spectra do not show the 500 cm^{-1} mode in the nominally $[a(bb)\bar{a}]$ polarized spectra, thus excluding a *bc* misalignment.

Fig. 10 displays a TEM micrograph of an *a*-axis oriented YBCO film. The most pronounced defects are APBs, which are likely to be caused by the underlying PBCO template. Due to the homoepitaxial growth of YBCO on PBCO, defect structures like APBs in the template layer will be continued into the YBCO layer. At the APBs the Ba rows turn into Y rows and the Cu rows remain undisturbed, resulting in a staggering of the domains by $c/3$ and $c/6$ along the (001) direction, just as in PBCO. *bc* twinning is nearly absent, well in agreement with our results from investigations on the in-plane orientation by XRD and Raman spectroscopy.

AFM images of the YBCO films reveal the same value of the mean surface roughness, $R_a = 5$ nm, as we have obtained for the PBCO templates.

4. Resistivity, T_c and critical current density

The anisotropic transport properties were characterized by four-point measurements of the resistivity and the critical current densities on thin, $d = 20$ nm, YBCO films. To this end we patterned the films into bridges of 400 μm length and 100 μm width by conventional photolithography, one bridge ||(001) LSGO, the other ||(010) LSGO, both oriented parallel to the edges of the substrate crystal. Gold contacts were sputtered ex situ using metal masks.

The temperature dependence of the resistivity is shown in Fig. 11(a). The onset of the transition temperature, T_c, is at 90.5 K in *b*- and *c*-direction with a transition width of 1.5 K (90% to 10% value). Inductive T_c measurements on unpatterned films yielded a T_c and ΔT_c of 89 and 3 K, respectively.

In the normal state, ρ_c increased with decreasing temperature, showing a semiconductor-like behavior, $d\rho_c/dT < 0$, of the form $\rho_c = A_c + B_c/T$, where $A_c = 25$ mΩ · cm and $B_c = 0.7$ Ω · cm K. ρ_b shows

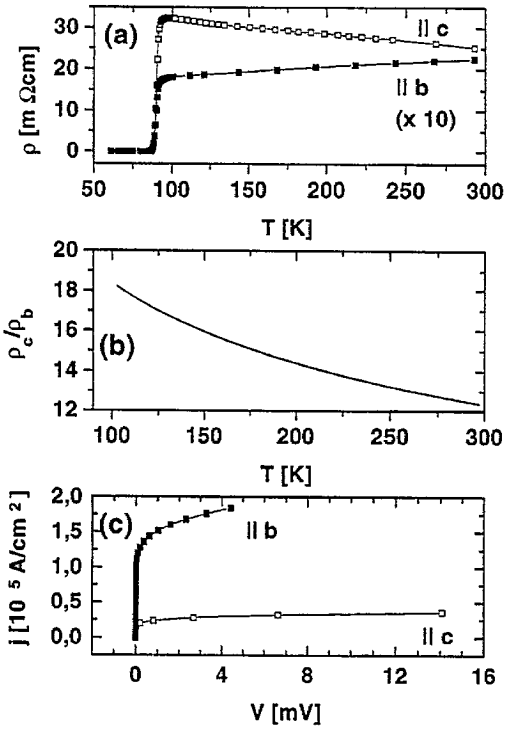

Fig. 11. (a) Resistivity versus temperature of a patterned YBCO film; (b) temperature dependence of the resistivity anisotropy, ρ_c/ρ_b, derived from fits of the normal state resistivities ρ_c and ρ_b, displayed in (a); (c) current densities versus voltage at 77 K.

a typical metal-like behavior of the form $\rho_b = A_b + B_b T$, where A_b, the zero-temperature intercept of the normal state resistivity, amounts to 1.5 mΩ · cm, and $B_b = 2.4$ μΩ · cm/K. The temperature dependence of the anisotropy of resistivity, ρ_c/ρ_b, displayed in Fig. 11(b), is therefore proportional to $1/T^2$, resulting in an anisotropy of 18 at 100 K and 12 at room temperature.

Although there is currently no consensus about the important mechanisms contributing to *c*-axis transport in high-temperature superconductors [42–45] a semiconducting-like behavior with $d\rho/dT < 0$ for ρ_c seems to be intrinsic [46]. ρ_c is often fitted with an expression of the form $\rho_c(T) = A_c T + B_c/T$, also proposed by many theoretical groups [42,43,45], where A_c and B_c can be interpreted as a measure of electrical separation of the Cu–O double layers. Batlogg et al. [46] have supposed that for an ideal crystal without dislocations, stacking faults and twinning a crosscontamination between *c*-axis and *ab*-

plane transport mechanisms will vanish, leading to a domination of the $1/T$ term. Resistivity measurements on single crystals by Hagen et al. [47] and Martin et al. [48] resulted indeed in a nearly pure $1/T$ temperature dependence of ρ_c and a linear behavior in T of ρ_b. The anisotropy of resistivity, ρ_c/ρ_b, depends therefore on $1/T^2$ as we have observed on our YBCO films. The authors have also obtained values for B_c between 0.6 and 1 $\Omega \cdot$ cm K and a residual resistivity around 10 m$\Omega \cdot$ cm.

There are likewise groups which propose a semiconducting-like behavior for ρ_c but only for underdoped or disordered samples [44,45]. The fact that we obtained T_c values of 90 K shows that our samples do only slightly differ from optimal doping. However, as we have seen from TEM micrographs, our YBCO films contain APBs which are probably caused by a Y/Ba cation disorder. So it is still open whether the $1/T$ temperature dependence of ρ_c is intrinsic or caused by some structural disorder.

Turning to the resistivity in b-direction, ρ_b, there are differences to literature concerning the parameters A_b and B_b. First, the slope $d\rho_b/dT$, B_b, of oriented thin films amounts typically to 0.6–0.7 $\mu\Omega \cdot$ cm/K. Our value is a factor of 4 larger. An increase of B_b is often observed in oxygen deficient YBCO films [21], however, in combination with a significant decrease of T_c, which does not occur in our samples. Second, the residual resistivity, A_b, is about one order of magnitude higher than reported values for a-axis oriented YBCO films on (100) LSGO [21]. This can possibly be explained in terms of planar defects, namely the observed APBs and SFBs. It is believed that they contribute to the residual resistivity [19], and they might be more pronounced in our films.

The measurements of the critical current densities $j_c \| b$ and $j_c \| c$ displayed in Fig. 11(c) were carried out at 77 K. The critical current density in b-direction, $j_c \| b$, reaches 1.3×10^5 A/cm^2 using a field criterion of 25 μV/cm. The anisotropy of the critical current densities, $j_c \| b / j_c \| c$, amounts to 7, which is significantly smaller than the anisotropy in resistivity.

Although $j_c \| b$ has a rather high value compared to those of standard a-axis oriented YBCO films, our value is still about one order of magnitude lower than the reported j_c values of c-axis oriented films. The reason for the strong decrease of $j_c \| b$ in a-axis oriented YBCO films is still unclear. Grain boundaries like APBs or (010)-basal-plane-faced tilt grain boundaries (BFGBs) as discussed in Ref. [49], are often believed to be the cause of the low critical current densities in conventional a-axis films. The mentioned grain boundaries do not show weak link behavior. As the authors have pointed out, they do not reduce $j_c \| b$ by more than one order of magnitude in consequence of their rather strong coupling [19]. A possible explanation for the reduced j_c in a-axis oriented films could be the absence of defects which act as pinning centers. The microscopic growth quality of a-axis oriented films is superior to that of c-axis films which often have many structural defects like oxygen vacancies (point defects) [50–52], grain boundaries [53,54], precipitates [55], growth steps on the film surface [56], dislocation chains in growth terraces [57] and others, representing possible pinning centers for magnetic flux lines.

5. Summary

High-quality 20 nm thick YBCO films with an a-axis content larger than 98% and a nearly full in-plane alignment of the c-axis, > 98%, were grown on (100) LSGO substrates using PBCO templates. We studied in detail optimal growth conditions for a-axis oriented YBCO and PBCO films. The quality of the YBCO films regarding their crystalline structure and superconducting properties can significantly be increased when a PBCO template is used. It is necessary to grow templates with a good in- and out-of-plane orientation, because these properties do chiefly limit the quality of the overlying a-axis oriented YBCO film.

The YBCO films showed good superconducting properties with an onset of T_c at 90.5 K and a transition width of $\Delta T_c = 1.5$ K. Resistivity measurements on patterned samples revealed a $1/T$ temperature dependence of ρ_c. Whether this results from planar structure defects, like APBs and SFs, or rather is an intrinsic behavior caused by a current path across possibly weakly linked Cu–O planes is still unclear and has to be investigated in more detail. ρ_b is linear in T with a relatively high residual resistivity of 1.5 m$\Omega \cdot$ cm which has been discussed in

terms of APBs. The anisotropy, ρ_c/ρ_b, was found to be proportional to $1/T^2$ amounting to 18 at 100 K.

Measurements of the critical current densities at 77 K resulted in a much smaller anisotropy, $j_c \| b / j_c \| c$, of about 7. $j_c \| b$ reaches 1.3×10^5 A/cm^2, which is high compared to standard a-axis oriented YBCO films, but still one order of magnitude smaller than reported values for c-axis oriented films.

Acknowledgements

This work was financially supported by the German ministry BMBF under Grant No. 13N6450, and the European Union (Esprit Project No. 8132 "WELITTD-HTS").

References

[1] D.K. Chim, T. van Duzer, Appl. Phys. Lett. 58 (1991) 753.
[2] O. Michikami, M. Asahi, Jpn. J. Appl. Phys. 30 (1991) 466.
[3] L.P. Lee, K. Char, M.S. Colclough, G. Zaharchuk, Appl. Phys. Lett. 59 (1991) 3051.
[4] A.H. Miklich, J.J. Kingsten, F.C. Wellstood, J. Clark, M.S. Colclough, K. Char, G. Zaharchuk, Appl. Phys. Lett. (1991) 988.
[5] J.M. Pond, K.R. Caroll, J.S. Horwitz, D.B. Crisey, M.S. Osofsky, V.C. Cestone, Appl. Phys. Lett. 59 (1991) 3033.
[6] C.B. Eom, J.Z. Sun, K. Yamamoto, A.F. Marshall, K.E. Luther, T.H. Geballe, S.S. Laderman, Appl. Phys. Lett. 55 (1989) 595.
[7] C.B. Eom, A.F. Marshall, S.S. Laderman, R.D. Jacowitz, T.H. Geballe, Science 249 (1990) 1549.
[8] D. Lew, Y. Suzuki, C.B. Eom, M. Lee, J.M. Triscone, T.H. Geballe, M.R. Beasley, Physica C 185 (1991) 2553.
[9] K. Char, M.R. Hahn, T.L. Hylton, M.R. Beasley, T.H. Geballe, A. Kapitulnik, IEEE Trans. Magn. 25 (1989) 2422.
[10] A. Inam, C.T. Rogers, R. Ramesh, L. Farrow, K. Remschnig, D. Hart, T. Venkatesan, Appl. Phys. Lett. 57 (1990) 2484.
[11] C. Tome-Rosa, G. Jakob, M. Maul, A. Walkenhorst, M. Schmitt, P. Wagner, P. Przyslupski, H. Adrian, Physica C 171 (1990) 231.
[12] S. Miyazawa, M. Mukaida, Appl. Phys. Lett. 64 (1994) 2160.
[13] R. Brown, V. Pendrick, D. Kalokitis, B.H.T. Chai, Appl. Phys. Lett. 57 (1990) 1351.
[14] S. Hontsu, J. Ishii, T. Kawai, S. Kawai, Appl. Phys. Lett. 59 (1991) 2886.
[15] A.W. Mc Connell, R.A. Hughes, A. Dabkowski, H.A. Dabkowska, J.S. Preston, J.E. Greedan, T. Timusk, Physica C 225 (1994) 7.
[16] K.H. Young, J.Z. Sun, Appl. Phys. Lett. 59 (1991) 2448.
[17] S. Hontsu, N. Mukai, J. Ishii, T. Kawai, S. Kawai, Appl. Phys. Lett. 61 (1991) 1134.
[18] M. Mukaida, S. Miyazawa, Appl. Phys. Lett. 63 (1993) 999.
[19] Y. Suzuki, D. Lew, A.F. Marshall, M.R. Beasley, T.H. Geballe, Phys. Rev. B. 48 (1993) 10642.
[20] W. Ito, Y. Yoshida, S. Mahajan, T. Morishita, Physica C 227 (1994) 313.
[21] Z. Trajanovic, I. Takeuchi, P.A. Warburton, C.J. Lobb, T. Venkatesan, Physica C 265 (1996) 79.
[22] A. Dabkowski, H.A. Dabkowska, J.E. Greedan, J. Cryst. Growth 132 (1993) 205.
[23] U. Jeschke, R. Schneider, G. Ulmer, G. Linker, Physica C 243 (1995) 243.
[24] M. Mukaida, S. Miyazawa, Y. Kobayashi, Proceedings of the ISS'92, Kobe, 1992, p. 893.
[25] S. Mahajan, J.G. Wen, W. Ito, C.H. Cho, T. Takenaka, N. Kubota, Y. Yoshida, T. Morishita, Physica C 225 (1994) 353.
[26] S. Mahajan, J.G. Wen, W. Ito, N. Kubota, C.J. Liu, T. Morishita, Appl. Phys. Lett. 65 (1994) 3129.
[27] T. Nagano, T. Hashimoto, J. Joshida, Physica C 265 (1996) 214.
[28] E. Sodtke, H. Münder, Appl. Phys. Lett. 60 (1992) 1630.
[29] G.J. Sung, J.D. Suh, Appl. Phys. Lett. 67 (1995) 1145.
[30] I. Takeuchi, P.A. Warburton, Z. Trajanovic, C.J. Lobb, Z.W. Dong, T. Venkatesan, M.A. Bari, W.E. Booij, E.J. Tarte, M.G. Blamire, Appl. Phys. Lett. 69 (1996) 112.
[31] S. Miyazawa, M. Mukaida, Jpn. J. Appl. Phys. 35 (1996) L1177.
[32] S.K. Streiffer, B.M. Lairson, E.M. Zielinski, J.C. Bravman, Phys. Rev. B 47 (1993) 11431.
[33] R. Ramesh, T.S. Ravi, D.M. Hwang, C.C. Chang, A. Inam, T. Venkatesan, X.D. Wu, R.E. Muenchhausen, S. Foltyn, N.S. Nogar, Physica C 173 (1991) 163.
[34] R. Ramesh, C.C. Chang, T.S. Ravi, D.M. Hwang, A. Inam, X.X. Xi, Q. Li, X.D. Wu, T. Venkatesan, Appl. Phys. Lett. 57 (1990) 1064.
[35] S.J. Pennycook, M.F. Chisholm, D.E. Jesson, R. Feenstra, S. Zhu, X.Y. Zheng, D.J. Lowndes, Physica C 202 (1992) 1.
[36] T. Burmann, J. Geerk, O. Meyer, R. Schneider, G. Linker, Solid State Commun. 90 (1994) 599.
[37] J.Q. Zheng, M.C. Shih, S. Williams, S.J. Lee, H. Kajiyama, X.K. Wang, Z. Zhao, K. Viani, S. Jacobson, P. Dutta, R.P.H. Chang, J.B. Ketterson, T. Roberts, R.T. Kampwirth, K.E. Gray, Appl. Phys. Lett. 59 (1991) 231.
[38] M. Mukaida, S. Miyazawa, Jpn. J. Appl. Phys. 32 (1993) 4521.
[39] J.G. Wen, S. Mahayan, W. Ho, T. Morishita, N. Noshizuka, Appl. Phys. Lett. 64 (1994) 3334.
[40] R. Schneider, J. Reiner, J. Geerk, O. Meyer, G. Linker, Solid State Commun. 89 (1994) 81.
[41] J.D. Jorgensen, M.A. Beno, D.G. Hinks, L. Soderholm, K.J. Volin, R.L. Hitterman, J.D. Grace, I.K. Schuller, C.U. Segre, K. Zhang, M.S. Kleefisch, Phys. Rev. B 36 (1987) 3608.
[42] Y. Zha, S.L. Cooper, D. Pines, Phys. Rev. B 53 (1996) 8253.
[43] N. Kumar, A.M. Jayannavar, Phys. Rev. B 45 (1992) 5001.

[44] A.G. Rojo, K. Levin, Phys. Rev. B 48 (1993) 16861.
[45] P.B. Littlewood, C.M. Varma, Phys. Rev. B 45 (1992) 12636.
[46] B. Batlogg, in: K.S. Bedell, D. Coffey, D. Meltzer, D. Pines, J.R. Schriffer (Eds.), High Temperature Superconductivity: The Los Alamos Symposium (1989), Addison-Wesley, Reading, MA, 1990, p. 37
[47] S.J. Hagen, T.W. Jing, Z.Z. Wang, J. Horvath, N.P. Ong, Phys. Rev. B 37 (1988) 7928.
[48] S. Martin, M. Gurvitch, C.E. Rice, A.F. Hebard, P.L. Gammel, R.M. Fleming, A.T. Fiory, Phys. Rev. B 39 (1989) 9611.
[49] D.J. Lew, Y. Suzuki, A.F. Marshall, T.H. Geballe, M.R. Beasley, Appl. Phys. Lett. 65 (1994) 1584.
[50] H. Theuss, H. Kronmüller, Physica C 177 (1991) 253.
[51] H. Theuss, Physica C 208 (1993) 155.
[52] R. Griessen, W. Hai hu, A.J.J. van Dalen, B. Dam, J. Rector, H.G. Schnack, Phys. Rev. Lett. 72 (1994) 1910.
[53] V.M. Pan, J. Alloys Compounds 195 (1993) 387.
[54] D.S. Misra, B.D. Padalia, S.P. Pai, R. Pinto, S.B. Palmer, Thin Solid Films 245 (1994) 186.
[55] O. Eibl, B. Roas, J. Mater. Res. 5 (1990) 2620.
[56] M. Mc Elfresh, T.G. Miller, D.M. Schaefer, R. Reifenberger, J. Appl. Phys. 71 (1992) 5099.
[57] R.M. Schalk, K. Kundzins, H.W. Weber, E. Stangl, S. Proyer, D. Bäuerle, Physica C 257 (1996) 341.